Available online at www.sciencedirect.com

SciVerse ScienceDirect

Ceramics International 38 (2012) 2355–2362

CERAMICS INTERNATIONAL

www.elsevier.com/locate/ceramint

Design of microwave dielectric resonator antenna using MZTO–CSTO composite

Shailendra Singh Rajput [a], Sunita Keshri [a,*], Vibha Rani Gupta [b], Nisha Gupta [b], Viktor Bovtun [c], Jan Petzelt [c]

[a] Department of Applied Physics, Birla Institute of Technology, Mesra, Ranchi 835215, India
[b] Department of Electronics and Communication Engineering, Birla Institute of Technology, Mesra, Ranchi 835215, India
[c] Department of Dielectrics, Institute of Physics, Academy of Sciences of the Czech Republic, Na Slovance 2, 18221 Praha 8, Czech Republic

Received 18 September 2011; accepted 31 October 2011
Available online 6 November 2011

Abstract

This paper presents the design of a cylindrical dielectric resonator antenna (DRA) using a nearly temperature stable dielectric composite material. By the combination of compounds with positive and negative temperature coefficient, a dielectric composite series $(1-x)(Mg_{0.95}Zn_{0.05})TiO_3 - x(Ca_{0.8}Sr_{0.2})TiO_3$ has been developed. The structural and morphological properties of the grown samples have been characterized by means of X-ray diffraction (XRD), scanning electron microscope (SEM) and energy dispersive X-ray (EDX) spectroscopy analysis. Microwave dielectric properties of the composite samples have been investigated using the $TE_{01\delta}$ dielectric resonator method. Relative permittivity (ε_r) of 21.9, dielectric loss tan δ of 0.0002 and temperature coefficient of resonant frequency (τ_f) of −0.15 ppm/°C have been obtained for the $x = 0.08$ sample, which was used for designing the DRA. The DRA resonates at 4.6 GHz frequency and offers the bandwidth of 315 MHz. The characteristics of proposed DRA have been simulated using the Ansoft high frequency structure simulator (HFSS). Comparison between the simulated and measured results shows a reasonably good agreement.

Keywords: B. Composites; Permittivity; Dielectric resonator antenna; Radiation pattern

1. Introduction

The dielectric resonators (DRs) have potential applications in microwave devices such as filters, duplexers, oscillators and patch antennas useful for cellular phones and global positioning systems capable of operating in the GHz range [1–7]. A DR consists of a block of dielectric material and can be of various geometrical shapes, e.g. cylindrical, rectangular, spherical and conical. The physical dimensions and permittivity of the dielectric block determine its resonant frequency. When a DR is not entirely enclosed by a conducting boundary, it can radiate and so it becomes an antenna, called dielectric resonator antenna (DRA). Although open DRs were found to radiate many years ago [3], in recent years the frequency range of interest has gradually progressed to the 3–30 GHz band. The DRAs are increasingly becoming attractive for many applications in wireless communication due to their interesting features like high radiation efficiency, compact size, low cost, compatibility with monolithic microwave integrated circuits (MMICs) and ability to obtain different radiation patterns by exciting different modes with different feeding mechanisms [1,2]. As the main body of the DRA is not made of metal, the loss would be greatly reduced when compared with some antenna designs consisting of mainly metallic structure, such as the patch antennas. The only loss for a DRA is that due to the imperfect dielectric material, which can be very small in practice. Thus DRA has found potential applications in the microwave, millimeter wave band and above.

For this type of applications, the dielectric materials must have the combined dielectric properties of a high permittivity (ε_r), a low dielectric loss (tan δ), a high quality factor ($Q \times f$) and a very small (~0) temperature coefficient of the resonant frequency (τ_f). The τ_f value is a measure of the drift in the resonant frequency with respect to temperature. Material

* Corresponding author. Tel.: +91 651 2275444; fax: +91 651 2275401.
E-mail addresses: s_keshri@bitmesra.ac.in, sskeshri@rediffmail.com (S. Keshri).

0272-8842/$36.00
doi:10.1016/j.ceramint.2011.10.088

having a large τ_f is not useful in a microwave circuit as it is difficult to maintain its resonant frequency with changes in the operating temperature [8], therefore its τ_f value should be close to zero for the thermal stability of the device [9,10]. Recently the use of dielectric composites has been proposed for controlling these properties. It has been observed that the mixing of two or more compounds with negative and positive temperature coefficients is the most promising method for obtaining a zero τ_f value [7,9]. The $MgTiO_3$-based ceramics are widely applied as dielectrics in resonators, filters and antennas for communication at microwave frequencies [7,11]. The $MgTiO_3$ ceramics show good dielectric properties: $\varepsilon_r \sim 17$, $Q \times f \sim 160{,}000$ GHz and a negative $\tau_f \sim -51$ ppm/°C [12]. The $CaTiO_3$ ceramics also show good dielectric properties: $\varepsilon_r \sim 170$, $Q \times f \sim 3600$ GHz and a large positive $\tau_f \sim 800$ ppm/°C [13]. From previous reports it was found that the $0.95MgTiO_3$–$0.05CaTiO_3$ ceramic exhibits the dielectric properties of $\varepsilon_r \sim 21$, $Q \times f \sim 56{,}00$ GHz, and $\tau_f \sim 0$ ppm/°C [14]. However, it required sintering temperatures as high as 1400–1500 °C. Many researchers made efforts to study the microstructures and the microwave dielectric properties of these ceramics by adding various additives, varying synthesis processes or by replacing Mg and Ca with suitable dopants [15–17]. Recently the $MgTiO_3$–$CaTiO_3$ ceramic composites with the partial replacement of Mg and Ca are found to show better microwave dielectric properties useful for dielectric resonators [16,17] and these can be synthesized at a lower sintering temperature (~1300 °C). The $(Mg_{0.95}Zn_{0.05})TiO_3$ (MZTO) ceramic was investigated to possess excellent dielectric properties with $\varepsilon_r \sim 16.21$, $Q \times f \sim 240{,}000$ GHz and a negative $\tau_f \sim -60$ ppm/°C [18,19]. Another ceramic $(Ca_{0.8}Sr_{0.2})TiO_3$ (CSTO), having dielectric properties of $\varepsilon_r \sim 181$, $Q \times f \sim 8300$ GHz and a large positive $\tau_f \sim 991$ ppm/°C [20], can be chosen as a τ_f compensator for MZTO.

Hence for achieving an effective compensation in its temperature coefficients, in present work CSTO has been added to MZTO with different percentages and a systematic study on the properties of a ceramic composite system $(1-x)$ MZTO $-$ (x)CSTO, with $x = 0.02$–0.08 have been carried out. It has been observed that CSTO addition increases the ε_r, decreases the quality factor ($Q \times f$ value), and compensates τ_f of MZTO. A cylindrical DRA has been designed using one of the compositions of this series which has a relatively high permittivity and a near-zero τ_f. The characteristic of designed antenna has been simulated using high frequency structure simulator (HFSS) based upon the finite element method (FEM), which characterizes the 3D designs. The variation of return loss versus frequency, the input impedance at resonant frequency and far field radiation patterns of the DRA are determined experimentally and compared with the simulated results.

2. Experimental

The $(1-x)$MZTO $-$ (x)CSTO, where $x = 0.02$, 0.03, 0.04, 0.05, 0.06 and 0.08 ceramic composites were prepared using the conventional solid state reaction method. At first MZTO and CSTO were separately synthesized from the raw materials $MgO/CaCO_3$, $ZnO/SrCO_3$ and TiO_2 powders by taking the stoichiometric amount of these as per requirement. The raw materials were accurately weighed and mixed with distilled water for 24 h in a ball mill using zirconia balls. The dried powder was calcined at 1100 °C for 4 h [15,17]. To get the composite samples of MZTO–CSTO series, the calcined powders of MZTO and CSTO were then mixed in desired ratio and remilled for 24 h. Polyvinyl alcohol (PVA) solution of 3 wt.% was added to the remilled product and pressed in the form of cylindrical pellets of diameter 8 mm and height 5 mm. These pellets were sintered at 1300 °C for 4 h in air. The apparent density of grown samples was measured by the Archimedes method. The crystalline structure of the samples were characterized by the X-ray diffraction (XRD; Philips, CuK_α radiation) with a step size of 0.02 in the range of $20^\circ \leq 2\theta^\circ \leq 80^\circ$ and scanning electron microscope (SEM; JEOL, Model: JSM-6390LV) equipped with energy dispersive X-ray (EDX) spectrometer (Oxford INCA, Model: DCL-7673).

Microwave dielectric properties of the composites were measured using the $TE_{01\delta}$ resonance mode of the cylindrical pallets inserted in a shielding cavity by Agilent PNA E8364B network analyzer in the transmission setup with a weak or moderate coupling [21,22]. The cavity with DR was placed in the Janis close-circle He cryostat, which allows temperature measurements in the interval of 10–380 K. Numerical calculations of the dielectric parameters from the measured resonance frequencies and Q-factors were based on the electrodynamic analysis [21,22]. For the study of antenna characteristics of the DRA, an Agilent PNA E8364B vector network analyzer (10 MHz–50 GHz, coaxial output 2.4 mm), signal generator (Rhode and Schwarz) and spectrum analyzer (Rhode and Schwarz) were used. The Ansoft HFSS software has been employed to simulate the DRA characteristic.

3. Results and discussion

3.1. Structural and dielectric properties

The XRD patterns of MZTO, CSTO and $(1-x)$ MZTO $-$ (x)CSTO, where $x = 0.02$–0.08 ceramics are shown in Fig. 1. It is seen from the figure that in the composite samples, MZTO presents as the main crystalline phase in association with minor phase of CSTO. With the increase in x, CSTO phase appeared gradually enhanced, and a two-phase system was clearly observed. The XRD peak indicated by '+' corresponds to the $(Mg_{0.95}Zn_{0.05})Ti_2O_5$ compound, which is difficult to completely eliminate from the sample prepared by mixed oxide route although it might affect the microwave dielectric properties of samples [12]. Other than this spurious peak, the diffraction peaks caused by the individual phases are distinguishable from each other indicating almost no chance of interdiffusion. By employing 'Checkcell' software it is observed that MZTO has a rhombohedral structure with lattice constants $a = 5.152(1)$ Å and $c = 13.856(1)$ Å having $R\bar{3}$ space group whereas the pure CSTO has an orthorhombic structure

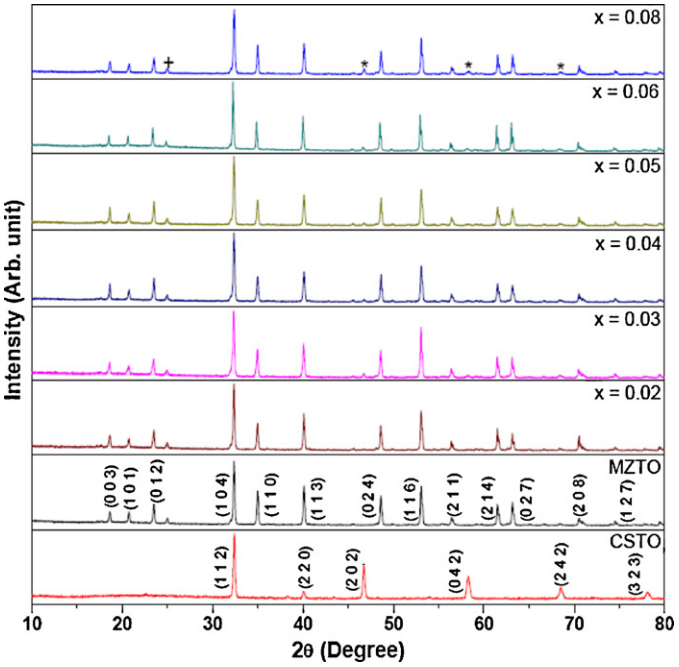

Fig. 1. XRD patterns of MZTO, CSTO and $(1-x)$MZTO $-$ (x)CSTO where $x = 0.02$, 0.03, 0.04, 0.05, 0.06 and 0.08 ceramic composites. [(+) $Mg_{0.95}Zn_{0.05}Ti_2O_5$, (*) $Ca_{0.8}Sr_{0.2}TiO_3$].

with lattice constants $a = 5.416(1)$ Å, $b = 5.439(1)$ Å, and $c = 7.684(2)$ Å having *Pbnm* space group.

The surface microstructural images of $(1-x)$ MZTO $-$ (x)CSTO, where $x = 0.02$–0.06 composites are shown in Fig. 2(a)–(e). The figures show compact distribution of grains of different shapes. All specimens show a similar surface morphology since the variation in their compositional ratio is small. Fig. 3(a)–(d) shows the SEM and EDX results of $x = 0.08$, *i.e.* 0.92MZTO–0.08CSTO sample. Fig. 3(b) explains the existence of elemental peaks corresponding to both the phases, which are found when we take EDX for entire sample area as shown in Fig. 3(a). Fig. 3(c) and (d) provides the EDX results corresponding to the spots 'A' and 'B' where the elemental peaks are found mainly of CSTO and MZTO phases, respectively. The peaks for Au have appeared because of the fact that the samples were coated by gold to avoid charging. From combined study of SEM and EDX, it has been understood that in this sample grains of both the phases are clearly distinguishable from each other and the CSTO grains are distributed randomly beside the MZTO grains.

Fig. 4 represents the relative permittivity (ε_r) and dielectric loss (tan δ) of $(1-x)$MZTO $-$ (x)CSTO composite samples in the microwave frequency range. From this figure it is evident that ε_r increases from 18.6 to 21.9 and tan δ also increases from 0.00009 to 0.0002, when the amount of CSTO addition increases from 0.02 to 0.08. This is because of the fact that CSTO has higher permittivity and loss compared to those of MZTO, hence samples of this series show a combined behaviour. From this figure it may be noticed that the loss of the $x = 0.03$ sample is relatively high which may be due to a higher part of some extrinsic losses compared to other samples. The $Q \times f$ and τ_f values of $(1-x)$MZTO $-$ (x)CSTO composites with the variation of CSTO percentage are demonstrated in Fig. 5. The $Q \times f$ value decreases with the CSTO addition because it is smaller for CSTO compared to that for MZTO. The τ_f values of the samples mainly depend on the composition(s) of the material and the spurious compound if any. It can be defined as follows:

$$\tau_f = \frac{f_2 - f_1}{f_2(T_2 - T_1)} \quad (1)$$

where f_1 and f_2 represent the resonant frequencies at two different temperatures T_1 and T_2, respectively. It is observed from the figure that the τ_f of $(1-x)$MZTO $-$ (x)CSTO ceramics rapidly changes with increasing x value due to a large positive τ_f of CSTO ($\tau_f \sim 991$ ppm/°C). It varies from -49.96 to -0.15 ppm/°C as the amount of CSTO addition increases from 0.02 to 0.08. A nearly zero τ_f ($\sim$0.15 ppm/°C) has been achieved for the 0.92MZTO–0.08CSTO sample. The values of ε_r, tan δ, $Q \times f$, τ_f and density of these samples have been listed in Table 1.

Temperature dependence of the relative permittivity changes gradually on increasing CSTO concentration (Fig. 6a) from the $MgTO_3$-like one with decreasing permittivity on cooling ($x = 0.02$ composition) to the $CaTiO_3$-like one with increasing permittivity on cooling ($x = 0.08$ composition). The competition of MZTO and CSTO component influence is better seen in the normalized $\varepsilon(T)$ plots (Fig. 6b). The "compensation point", corresponding to the $\varepsilon(T)$ minimum, shifts from 70 K to 330 K on increasing the CSTO component. For 0.92MZTO–0.08CSTO sample this point is close to the room temperature, consequently this composition is characterized by the best stability of the microwave dielectric parameters at working temperatures.

Microwave dielectric losses increase on increasing CSTO concentration (Fig. 7) at all studied temperatures (Fig. 7). A tan $\delta(T)$ maximum is observed near 100 K for all the compositions, which indicates a weak dielectric relaxation passing through the GHz range at this temperature. The value of tan $\delta(T)$ maximum increases monotonically with the CSTO concentration which means that it is due to this component. It should be considered that CSTO, as well as CTO is orthorhombic and ferroelastic [23,24]. Presence of the possible ferroelastic domains could result in weak relaxation processes producing additional dielectric losses. But due to its weakness, no measurable contribution to permittivity was observed. The microwave losses remain still very low at all the temperatures and bring no limitations for the tentative applications of the MZTO–CSTO composites.

3.2. Properties of designed DRA

We have designed a cylindrical DRA using the 0.92MZTO–0.08CSTO sample, because a nearly zero value of τ_f ensures the stability of the microwave components at different working temperatures. The cylindrical DRA offers greater design flexibility compared to different other shapes of DRA, as in this case the ratio of radius to height (a/h) controls the resonant

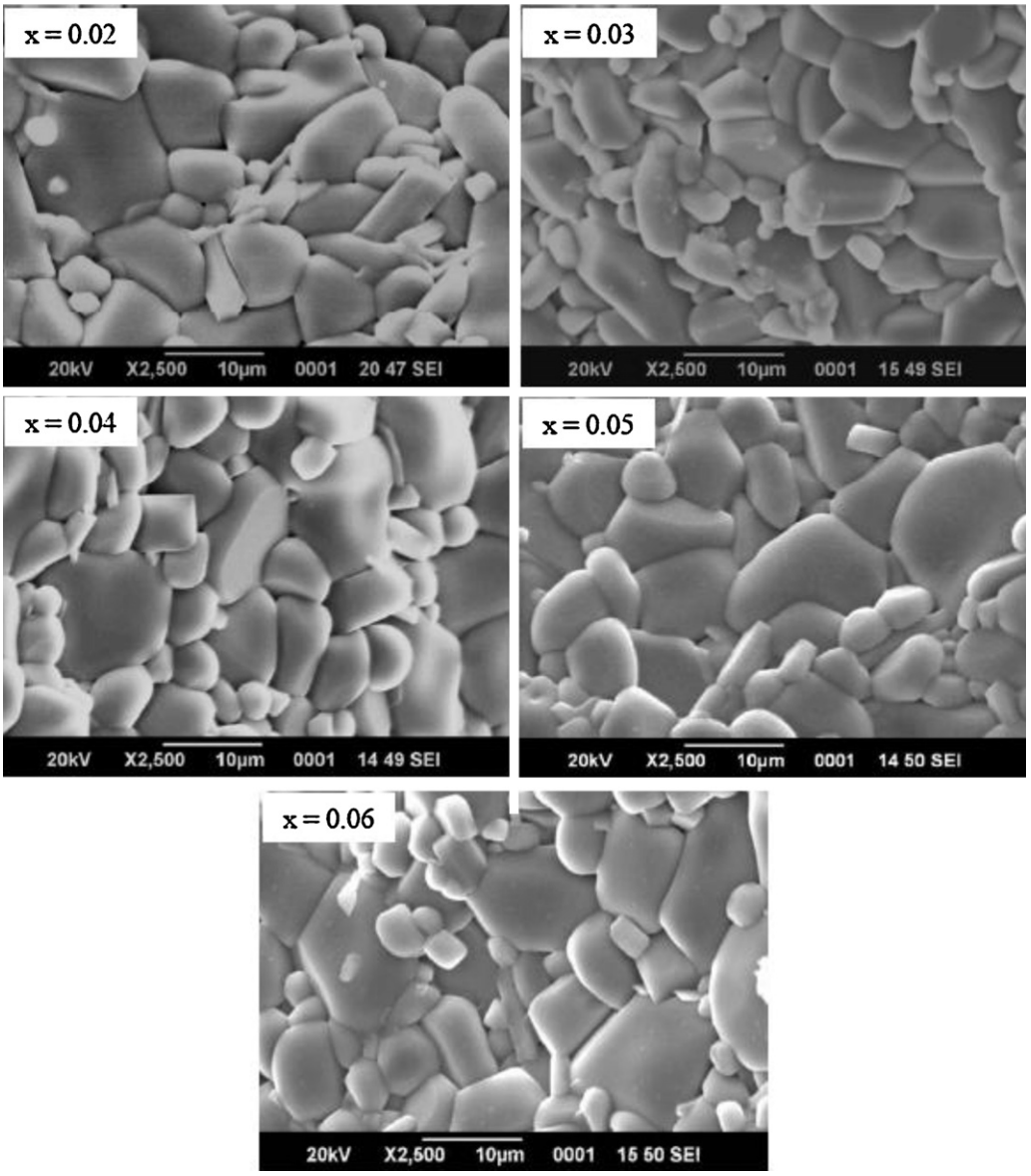

Fig. 2. SEM micrographs of the $(1-x)$MZTO $-$ (x)CSTO ceramic composites sintered for 4 h at 1300 °C, (a) $x = 0.02$, (b) $x = 0.03$, (c) $x = 0.04$, (d) $x = 0.05$ and (e) $x = 0.06$.

frequency and the Q factor. Fabrication is also simpler than for others. In order to determine the bandwidth and the radiation patterns of the designed DRA, the properties of this DRA has been studied by performing experiment as well as simulation. The DRA is placed above a conducting ground plane made of copper plate and excited by a coaxial probe feed with varying probe length of SMA connector. The outer conductor of subminiature version A (SMA) connector is connected to the ground plane and the inner conductor (probe) is connected to the DRA as shown in Fig. 8(a) and (b). The ground plane often affects the radiation properties of the antenna and it is important to be able to predict such variation. When a DRA is excited with a coaxial probe feed, the electric field (E) lines terminate usually to the surface of the feed probe. Since the normal component of E is discontinuous across a surface separating two media of different permittivites, the introduction of a thin air gap between the feed probe and a dielectric resonator is considered in the DRA configuration [25]. The parameters that affect the overall performance of the antenna include the probe length of SMA connector, permittivity of the DRA, dimensions of the DRA, air gap between the probe and dielectric resonator and size of the ground plane. The length and width of the ground plane is optimized for maximum bandwidth operation of the antenna. The position of DRA on the ground plane is adjusted to obtain maximum bandwidth and better impedance matching. The simulation is repeatedly performed for different probe lengths of coaxial probe and also for its different positions. After thorough studies with the help of simulations as well as experiment, it is observed that the probe length 0.65 cm and ground plane of dimensions $10\ \text{cm} \times 10\ \text{cm} \times 0.2\ \text{cm}$ offers reasonably good agreement between the simulated and measured results. The cylindrical DRA, designed for this work has a radius $a = 0.645$ cm, height $h = 0.729$ cm and $\varepsilon_r = 21.9$ as shown in Fig. 8(b). The frequency at which the return loss of a

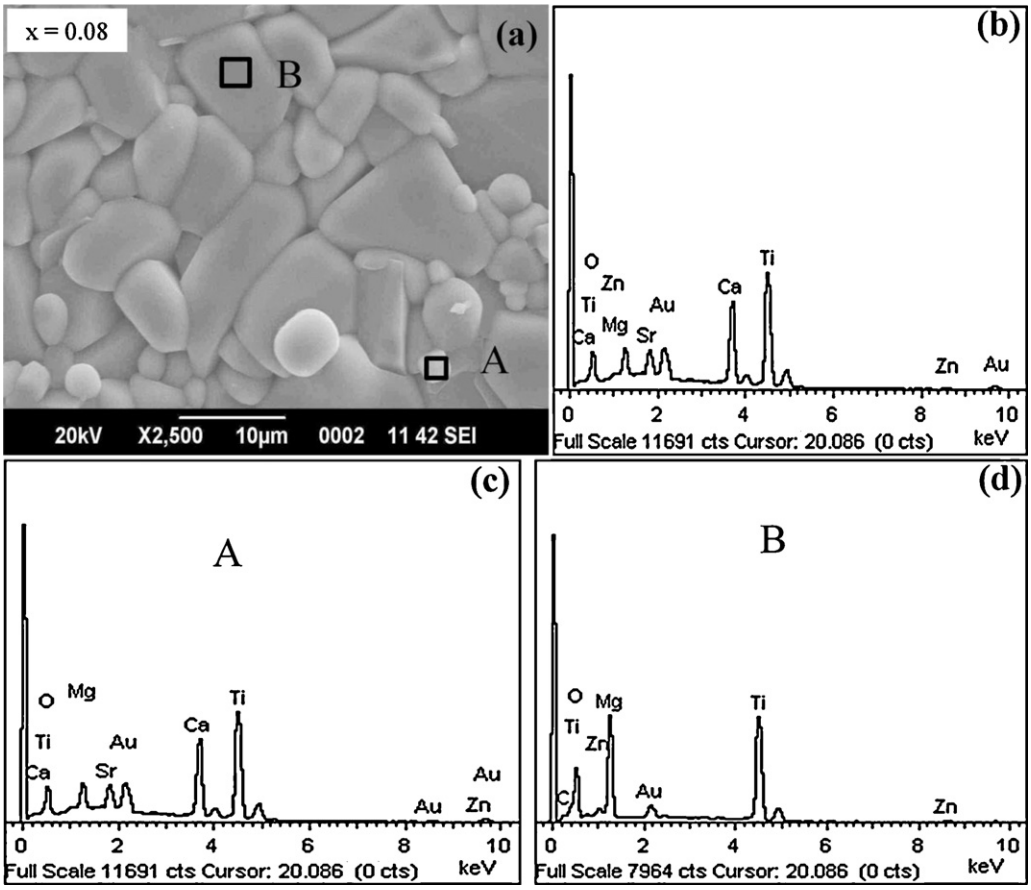

Fig. 3. (a) SEM image of 0.92MZTO–0.08CSTO sample, (b–d) EDX results of 0.92MZTO–0.08CSTO sample for entire area and positions 'A' and 'B', respectively.

DRA becomes minimum is called resonant frequency of the structure. The cylindrical DRA is worked at the $HEM_{11\delta}$ mode and its resonant frequency f_0 can be approximated by the following equation [3,26,27]:

$$f_0 = \frac{2.997}{20\pi\sqrt{2+\varepsilon_r}}\left[0.27 + 0.36\frac{a}{2h} + 0.02\left(\frac{a}{2h}\right)^2\right] \quad (2)$$

where ε_r is the relative permittivity, a and h are the radius and thickness of the DRA.

The simulated and measured variations of return loss versus frequency for the DRA are shown in Fig. 9. The resonant frequency of DRA has been measured at 4.6 GHz as compared to 4.55 GHz in the computations; *i.e.*, a marginal difference of 1.1% has been observed between the two sets of results. However, some deviations are observed in the simulated and measured values of return loss bandwidth. The resonant frequency of proposed DRA offers a bandwidth of 315 MHz (4.45–4.77 GHz) while 100 MHz bandwidth has been observed

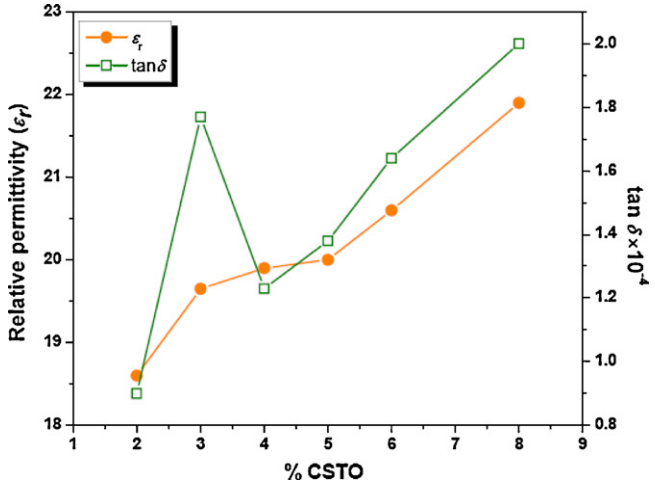

Fig. 4. Relative permittivity and loss factor of MZTO–CSTO composites as a function of CSTO addition.

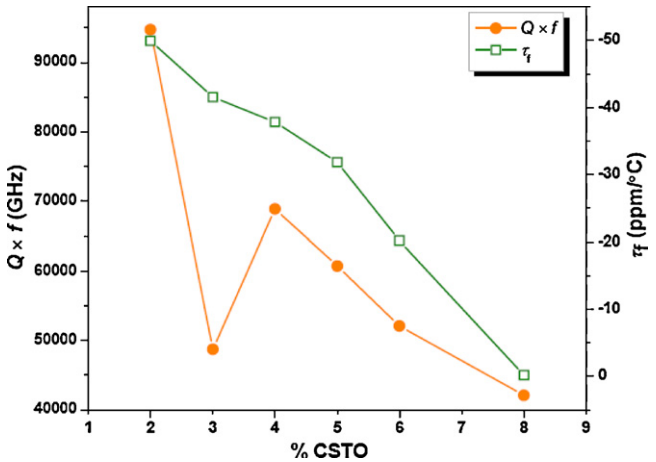

Fig. 5. $Q \times f$ values and τ_f values of MZTO–CSTO composites as a function of CSTO addition.

Table 1
The values of ε_r, tan δ, $Q \times f$, τ_f and density of MZTO–CSTO composites.

%CSTO	ε_r	Tan δ	$Q \times f$	τ_f	Density (gm/cm^3)
2	18.6	9E−5	94711.76	−49.96	3.73
3	19.65	1.77E−4	48736.8	−41.54	3.70
4	19.9	1.23E−4	68889.6	−37.83	3.73
5	20	1.38E−4	60711	−31.82	3.74
6	20.6	1.64E−4	52086	−20.18	3.77
8	21.9	2E−4	42080	−0.15	3.79

in the simulation. The difference may be due to the consideration of the finite size of ground plane during experiment and the edge diffraction effects [2,28,29]. The corresponding Smith chart representation of the S_{11} from 4.48 to 4.63 GHz is shown in Fig. 10. To obtain a low return loss at resonant frequency, the impedance locus should be shifted as near as possible to the center of the Smith chart. As seen from the measurement results, the input impedance is $47.85 - j29.99\ \Omega$ at the frequency of 4.55 GHz. A matching point is near the point of 4.6 GHz, which is very close to the center of the Smith chart.

The far field radiation patterns of the DRA for $\Phi = 0^\circ$ (E-plane) and $\Phi = 90^\circ$ (H-plane) have been measured at the respective resonant frequency of the antenna and compared with the simulated results; the results are presented in Fig. 11. The simulated and measured far field radiation patterns of the DRA for $\Phi = 0^\circ$ (E-plane) are in good agreement and show almost omni–directional characteristic. However, the simulated and measured results of radiation patterns for $\Phi = 90^\circ$ (H-plane) are not very similar. The difference between the results might have occurred because of the experimental errors associated with the positioning of feed cable with respect to orientation of the DRA. From the above studies it is observed that the expected resonant frequency can be obtained by

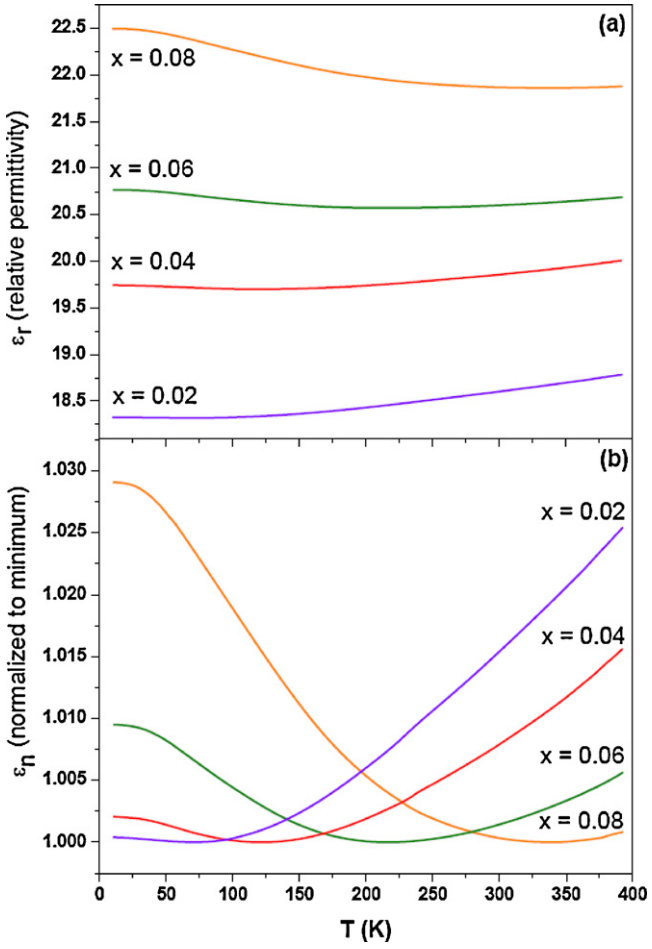

Fig. 6. Temperature dependences of the relative dielectric permittivity ε_r (a) and normalized permittivity ε_n (b) of $(1-x)$MZTO − (x)CSTO MZTO–CSTO composites for $x = 0.02$, 0.04, 0.06, and 0.08.

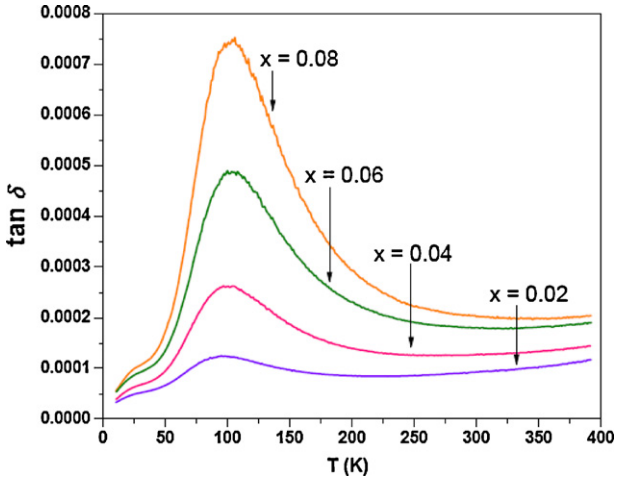

Fig. 7. Temperature dependences of the loss factor of composites for $x = 0.02$, 0.04, 0.06, and 0.08.

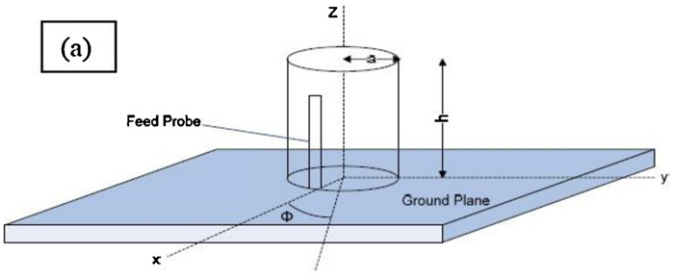

Fig. 8. (a) The geometry of the cylindrical DRA and (b) original DRA fabricated in lab.

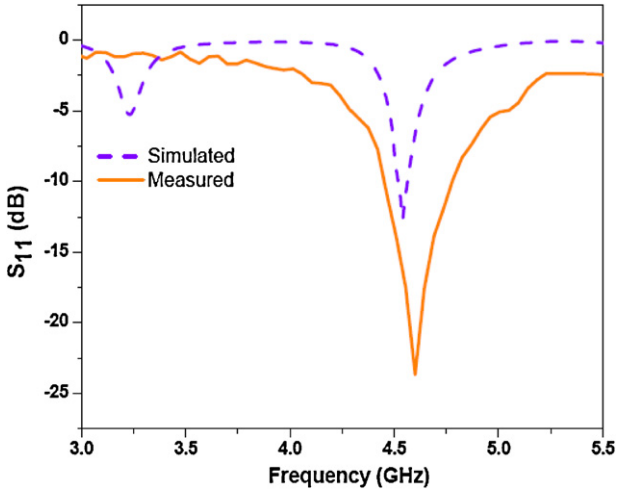

Fig. 9. Frequency dependent return loss of cylindrical DRA fabricated using 0.92MZTO–0.08CSTO material.

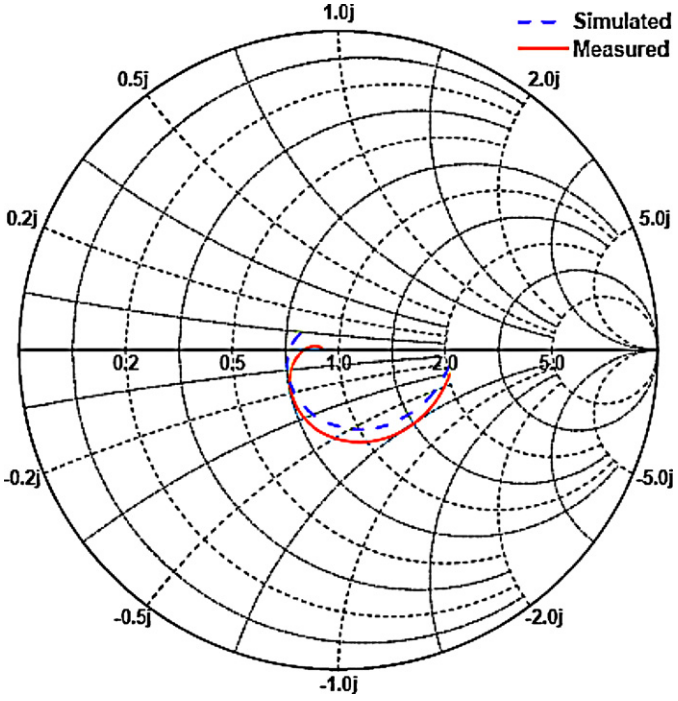

Fig. 10. Simulated and measured input impedance (Smith chart) of the DRA.

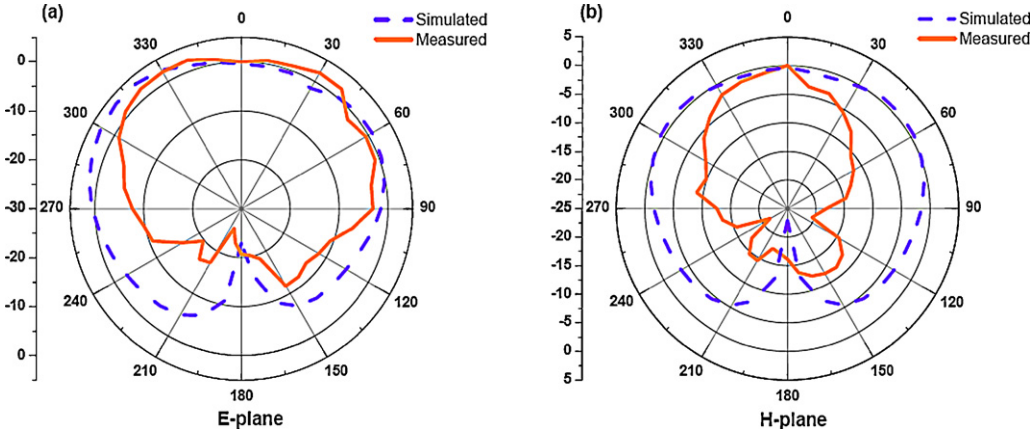

Fig. 11. Simulated and measured far field radiation patterns of the DRA for (a) $\Phi = 0^\circ$, (b) $\Phi = 90^\circ$ at 4.6 GHz.

choosing the dielectrics of suitable permittivity and size, and also having a near zero temperature coefficient of the resonant frequency. The results obtained here are encouraging and carry message that these types of DRAs can have practical applications in the radar communication field.

4. Conclusions

In this paper we report the microwave dielectric properties of $(1-x)$MZTO $-$ (x)CSTO dielectric composite series. The 0.92MZTO–0.08CSTO sample of this series is found to possess microwave dielectric parameters suitable for designing an antenna; its ε_r, $\tan\delta$ and τ_f are 21.9, 0.0002, and -0.15 ppm/°C, respectively. We have designed a cylindrical DRA using this material, which shows resonant frequency at 4.6 GHz with a bandwidth of 315 MHz. The characteristics of the proposed DRA have been simulated using the HFSS software and also studied through experiment. The agreement between the simulated and measured results is reasonably good. The results of the present report lead to the conclusion that such DRAs can be used as suitable candidates for the C-band (4–8 GHz) of radar frequency range.

Acknowledgements

The authors (S. Keshri, V. R. Gupta and N. Gupta) gratefully acknowledge Department of Science and Technology (DST), India for financial assistance. S.S. Rajput gratefully acknowledges DST, India for providing fellowship. The work was also supported by the Academy of Sciences of the Czech Republic (project AVOZ10100520).

References

[1] S.A. Long, M.W. McAllister, L.C. Shen, The resonant dielectric cavity antenna, IEEE Trans. Antenn. Propag. Ap–31 (1983) 406–412.

[2] A. Petosa, A. Ittipiboon, Y.M.M. Antar, D. Roscoe, M. Cuhaci, Recent advances in dielectric–resonator antenna technology, IEEE Antenn. Propag. Mag. 40 (1998) 35–48.

[3] K.M. Luk, K.W. Leung, Dielectric Resonator Antennas, Research Studies Press Ltd., Baldock, England, 2002.

[4] P.V. Bijumon, S.K. Menon, M.N. Suma, M.T. Sebastian, P. Mohanan, Broadband cylindrical dielectric resonator antenna excited by modified microstrip line, Electron. Lett. 41 (2005) 385–387.

[5] A.J. Moulson, J.M. Herbert, Electroceramics, second ed., Chapman and Hall, London, 1990.

[6] A.A. Kishk, H.A. Auda, B.C. Ahn, Radiation characteristics of cylindrical dielectric resonator antennas with new applications, IEEE Antenn. Propag. Soc. Newslett. 31 (1989) 7–16.

[7] Y.C. Chen, S.M. Tsao, C.S. Lin, S.C. Wang, Y.H. Chien, Microwave dielectric properties of $0.95MgTiO_3$–$0.05CaTiO_3$ for application in dielectric resonator antenna, J. Alloys Compd. 471 (2009) 347–351.

[8] M.T. Sebastian, K.P. Surendran, Tailoring the microwave dielectric properties of $Ba(Mg_{1/3}Ta_{2/3})O_3$ ceramics, J. Eur. Ceram. Soc. 26 (2006) 1791–1799.

[9] C.L. Huang, K.H. Chiang, Dielectric properties of B_2O_3-doped $(1-x)LaAlO_3 - xSrTiO_3$ ceramic system at microwave frequency, Mater. Res. Bull. 37 (2002) 1941–1948.

[10] L. Wu, Y.C. Chen, L.J. Chen, Y.P. Chou, Y.T. Tsai, Preparation and microwave characterization of $Ba_xSr_{1-x}TiO_3$ ceramics, Jpn. J. Appl. Phys. 38 (1999) 5612–5615.

[11] T.S. Rao, V.R.K. Murthy, B. Viswanathan, Review of perovskite ceramics—microwave dielectric resonator materials, Ferroelectrics 102 (1990) 155–160.

[12] K. Wakino, Recent development of dielectric resonator materials and filters in Japan, Ferroelectrics 91 (1989) 69–86.

[13] R.C. Kell, A.C. Greenham, G.C.E. Olds, High-permittivity temperature-stable ceramic dielectrics with low microwave, J. Am. Ceram. Soc. 56 (1973) 352–354.

[14] A. Belous, O. Ovchar, D. Durylin, M. Valant, M.M. Krzmancc, D. Suvorov, Microwave composite dielectrics based on magnesium titanates, J. Eur. Ceram. Soc. 27 (2007) 2963–2966.

[15] C.L. Huang, G.J. Li, J.J. Wang, Microwave dielectric properties of $(1\ x)(Mg_{0.95}Zn_{0.05})TiO_3\ x(Na_{0.5}La_{0.5})TiO_3$ ceramic system, J. Alloys Compd. 472 (2009) 497–501.

[16] V.M. Ferreira, F. Azough, R. Freer, J.L. Baptista, The effect of Cr and La on $MgTiO_3$ and $MgTiO_3$–$CaTiO_3$ microwave dielectric ceramics, J. Mater. Res. 12 (1997) 3293–3299.

[17] C.L. Pan, C.H. Shen, P.C. Chen, T.C. Tan, Characterization and dielectric behavior of a new dielectric ceramics $MgTiO_3$–$Ca_{0.8}Sr_{0.2}TiO_3$ at microwave frequencies, J. Alloys Compd. 503 (2010) 365–369.

[18] M.L. Hsieh, L.S. Chen, S.M. Wang, C.H. Sun, M.H. Weng, M.P. Houng, S.L. Fu, Low-temperature sintering of microwave dielectrics $(Zn,Mg)TiO_3$, Jpn. J. Appl. Phys. 44 (2005) 5045–5048.

[19] H.T. Kim, J.D. Byun, Y. kim, Microstructure and microwave dielectric properties of modified zinc titanates (II), Mater. Res. Bull. 33 (1998) 975–986.

[20] P.L. Wise, I.M. Reaney, W.E. Lee, T.J. Price, D.M. Iddles, D.S. Cannell, Structure–microwave property relations in $(Sr_xCa(1-x))_{n+1}Ti_nO_{3n+1}$, J. Eur. Ceram. Soc. 21 (2001) 1723–1726.

[21] J. Krupka, K. Derzakowski, B. Riddle, J. Baker-Jarvis, A dielectric resonator for measurements of complex permittivity of low loss dielectric materials as a function of temperature, Meas. Sci. Technol. 9 (1998) 1751–1756.

[22] J. Krupka, Frequency domain complex permittivity measurements at microwave frequencies, Meas. Sci. Technol. 17 (2006) R55–R70.

[23] A. Pashkin, S. Kamba, M. Berta, J. Petzelt, G.D.C. Csete de Györgyfalva, H. Zheng, H. Bagshaw, I.M. Reaney, High frequency dielectric properties of $CaTiO_3$-based microwave ceramics, J. Phys. D: Appl. Phys. 38 (2005) 741–748.

[24] V.Z. Elezny, E. Cockayne, J. Petzelt, M.F. Limonov, D.E. Usvyat, V.V. Lemanov, A.A. Volkov, Temperature dependence of infrared-active phonons in $CaTiO_3$: a combined spectroscopic and first-principles study, Phys. Rev. B 66 (2002), 224303 (1–12).

[25] G.P. Junker, A.A. Kishk, A.W. Glisson, D. Kajfez, Effect of an air gap around the coaxial probe exciting a cylindrical dielectric resonator antenna, Electron. Lett. 30 (1994) 177–178.

[26] D. Kajfez, P. Guillon, Dielectric Resonators, Artech House Publishers, London, 1986.

[27] A.A. Kishk, A.W. Glisson, D. Kajfez, Computed resonant frequency and far fields of isolated dielectric discs, IEEE Antenn. Propag. Soc. Int. Symp. Dig. (1993) 408–411.

[28] R.G. Kouyoumjian, P.H. Pathak, A uniform geometrical theory of diffraction for an edge in a perfectly conducting surface, Proc. IEEE 62 (1974) 1448–1461.

[29] A. Petosa, Dielectric Resonator Antenna Handbook, Artech House Publishers, US, 2007.